Rock Mechanics and Rock Engineering

A microplane-based anisotropic damage model for deformation and fracturing of brittle rocks

--Manuscript Draft--

Manuscript Number:	RMRE-D-22-01330R1
Full Title:	A microplane-based anisotropic damage model for deformation and fracturing of brittle rocks
Article Type:	Original Paper
Keywords:	brittle rocks; anisotropy; microplane model; numerical simulation; Intermediate principal stress; fracture pattern
Corresponding Author:	Tao Xu Northeastern University Shenyang, CHINA
Corresponding Author Secondary Information:	
Corresponding Author's Institution:	Northeastern University
Corresponding Author's Secondary Institution:	
First Author:	Yang Yuan
First Author Secondary Information:	
Order of Authors:	Yang Yuan
	Tao Xu
	Philip G. Meredith
	Thomas M. Mitchell
	Michael J. Heap
	Guanglei Zhou
	Ashley Stanton-Yonge Sesnic
Order of Authors Secondary Information:	
Funding Information:	National Natural Science Foundation of China (42172312, 51974062, 52211540395) — Prof. Tao Xu
	Royal Society Newton Mobility Grant (170625) — Prof Philip G. Meredith
Abstract:	Anisotropy is an important property that is widely present in crustal rocks. Efforts have been devoted to providing a constitutive model that can describe both inherent and stress-induced anisotropy in rock. Different from classic models, that are based on stress invariants or strain tensors, we propose here an anisotropic damage microplane model to capture the characteristics of rock properties in different orientations (i.e. their anisotropy). The basic idea is to couple continuum damage mechanics with the classic microplane model. The stress tensor in the model is dependent on the integration of microplane stresses in all orientations. The damage state of any element in the model is determined by the microplane that satisfies the maximum tensile stress criterion or Mohr-Coulomb criterion. An ellipsoidal function was used to characterize the failure strength, where the orientation of the failure plane changes with the preferred orientation of defects in the rock. The proposed model is validated against laboratory experiments performed on brittle material with orientated cracks and granite under true triaxial compression. The fracture pattern and the effect of the intermediate principal stress are numerically predicted by our anisotropic damage model, and we discuss relationships between the damage evolution and the anisotropy of the rock under true triaxial compression. The proposed numerical model, based on microplane theory,

A microplane-based anisotropic damage model for deformation and fracturing of brittle rocks

Yang Yuan[1], Tao Xu[1*], Philip G. Meredith[2], Thomas M. Mitchell[2], Michael J. Heap[3, 4], Guanglei Zhou[5], Ashley Stanton-Yonge Sesnic[2]

[1] *Center for Rock Instability and Seismicity Research, Northeastern University, Shenyang, 110819, China*

[2] *Department of Earth Sciences, University College London, London, WC1E 6BT, UK*

[3] *Université de Strasbourg, CNRS, Institut Terre et Environnement de Strasbourg, UMR 7063, 5 rue René Descartes, Strasbourg F-67084, France*

[4] *Institut Universitaire de France (IUF), 1 rue Descartes, Paris 75231, France*

[5] *College of Energy and Mining Engineering, Shandong University of Science and Technology, Qingdao, Shandong, 266590, China*

**Corresponding author: Tao Xu (xutao@mail.neu.edu.cn)*

Highlights

- Microplane-based anisotropic damage model incorporating maximum tensile stress criterion and Mohr-Coulomb criterion is proposed.
- Peak strength and elastic modulus vary with the preferred crack/damage angles.
- Fracture pattern of brittle rock and the effect of intermediate principal stress in true triaxial compressive tests is numerically replicated.

Abstract

Anisotropy is an important property that is widely present in crustal rocks. Efforts have been devoted to providing a constitutive model that can describe both inherent and stress-induced anisotropy in rock. Different from classic models, that are based on stress invariants or strain tensors, we propose here an anisotropic damage microplane model to capture the characteristics of rock properties in different orientations (i.e. their anisotropy). The basic idea is to couple continuum damage mechanics with the classic microplane model. The stress tensor in the model is dependent on the integration of microplane stresses in all orientations. The damage state of any element in the model is determined by the microplane that satisfies the maximum tensile stress criterion or Mohr-Coulomb criterion. An ellipsoidal function was used to characterize the failure strength, where the

orientation of the failure plane changes with the preferred orientation of defects in the rock. The proposed model is validated against laboratory experiments performed on brittle material with orientated cracks and granite under true triaxial compression. The fracture pattern and the effect of the intermediate principal stress are numerically predicted by our anisotropic damage model, and we discuss relationships between the damage evolution and the anisotropy of the rock under true triaxial compression. The proposed numerical model, based on microplane theory, offers a new approach to analyzing the effect of crack orientation on the deformation and fracture of brittle rock.

Keywords: Brittle rocks, anisotropy, microplane model, numerical simulation, intermediate principal stress, fracture pattern

Notation

$\varepsilon_{ij}, \sigma_{ij}$	Strain and stress tensor
$\varepsilon_N, \varepsilon_T$	Normal and tangential strain in microplane
$\varepsilon_M, \varepsilon_L$	Two components of the tangential strain in microplane
n_i, n_j	Unit normal vector, $i, j = 1,2,3$.
l_i, l_j, m_i, m_j	Components of unit tangential vector, $i, j = 1,2,3$.
E_N, E_T	Normal and tangential elastic modulus
v	Poisson's ratio
Ω	Surface of unit sphere
k, kth	Microplane number
ω_k	Integration weights of kth microplane
N_m	Total number of microplanes
u	Scale parameter of elements
u_0	Average parameter of elements
w	Heterogeneity index
σ_N^k, σ_T^k	Normal stress and tangential stress of kth microplane
σ_{t0}, σ_{c0}	Ultimate tensile strength and compression strength
S_0	Ultimate strength of element
θ_f, c_0	Friction angle and cohesion
E, E'	Undamaged and effective elastic modulus
D, D_t, D_c	Damage variable, tensile damage, shear damage under compression
$\varepsilon_{t0}, \varepsilon_{c0}$	Ultimate strain corresponding to the σ_{t0} and σ_{c0}
η	Residual strength coefficient (RSC)
AC, a, b, c	Anisotropy coefficient
θ_x	Angle between the preferred orientation and X-axis

1. Introduction

When a rock is stressed, microcracks can nucleate within or between the grains or crystals forming the rock. If the stress on the rock is increased further, these microcracks can extend and coalesce, eventually forming a macroscopic fracture that results in rock failure (Sammis and Ashby 1986, Ashby and Sammis 1990). The microcracks that grow in response to an applied stress are typically aligned parallel or subparallel to the direction of the maximum principal stress, progressively creating an anisotropy within the rock (Menéndez et al. 1996, Wu et al. 2000, Rizzo et al. 2018). The anisotropy that develops in response to differential loading may also be influenced by any preexisting anisotropy in the rock, such as a bedding, laminations, foliations, a preferred orientation of preexisting microcracks, or a grain or pore shape preferred orientation (Nara and Kaneko 2006). For example, a pore shape preferred orientation has been shown to influence the angle of compaction bands that form in porous volcanic rock (Heap et al. 2022).

The presence of microcracks reduces elastic wave velocities (O'Connell and Budiansky 1974). Thus, the development of an anisotropic network of microcracks (opening, closure, or shear displacement) can be monitored by measuring variations in elastic wave velocities (Schubnel and Guéguen 2003, Schubnel et al. 2006). This method has been previously used to monitor damage in, for sample, sandstone (Sayers et al. 1990, Sayers and Munster 1991, Shirole et al. 2020), granite (Benson et al. 2006), limestone (Gupta 1973), and serpentinites (David et al. 2018). The development of a microcrack anisotropy is more pronounced in experiments in which the stress is not applied hydrostatically (i.e. a differential stress) (Stuart et al. 1993, Browning et al. 2017, Browning et al. 2018). Rock is also considered to demonstrate a stress-memory effect (such as the so-called Kaiser effect; Lavrov 2003, Daoud et al. 2020), in which acoustic emissions (AE; commonly used as a proxy for the initiation of microcracks) are only observed in any stress cycle once the maximum stress in the previous cycle has been exceeded (Lavrov 2001, Heap et al. 2009, 2010, Cerfontaine and Collin 2018, Daoud et al. 2020). However, the rotation of the principal stress in cyclic, sequential, true triaxial loading tests (CSTT) leads to new AE output at lower stress levels than previously observed. These new microcracks are not randomly orientated and their orientation depends on the direction of the maximum compressive stress. Thus, it could be considered unsuitable to analyze the damage of brittle rock according to stress invariants (Browning et al. 2018).

A second-rank and fourth-rank crack density tensor can characterize anisotropic crack networks in rock and fit elastic wave velocity data (Sayers and Kachanov 1995). Phenomenological models and micromechanical approaches are two families of damage models that have been developed for the description of induced damage. The concept of continuum damage mechanics based on the principle of effective stress was introduced using a scalar damage variable. However, in phenomenological models, it is necessary to introduce vector or tensor damage variables to reflect anisotropic damage. To this end, Murakami (1983) extended the theory to describe the anisotropic creep damage state using a second rank symmetric damage tensor. Chow and Wang (1987) used a symmetric fourth rank tensor by taking anisotropic continuum damage into account in the principal coordinate system. In element-based modelling it is intuitive to provide a measure of element surface area change during deformation, which can be defined as the ratio of the damaged part of the element in the model to the total area. Macroscopic damage models based on a thermodynamic framework also present an attractive approach to model anisotropic damage development. Pellet et al. (2005), for example, replaced the scalar damage variable with a second rank tensor and introduced an anisotropic parameter β to describe the behavior of anisotropic viscoplastic rock based on Lemaitre's model. Shao et al. (2006) focused on the modeling of induced anisotropic damage during external loading and defined the macroscopic damage tensor as the variation of crack density in each orientation. However, it is challenging to capture damage orientation using stress and strain tensors with orthotropic invariants. In contrast, micromechanical approaches use the idea of a representative volume element (RVE) to study elastic solids containing inclusions, cavities, or cracks (Nemat-Nasser and Hori 2013). A microscopic-based model to describe the process of microcrack initiation, propagation, and the time dependent behavior of brittle-elastic rock under compression was constructed by Kachanov (1982a, 1982b, 1982c). The model of Kachanov (1982a, 1982b, 1982c) can consider frictional sliding and branched microcracks, and the averaging of crack orientations described the stress-induced anisotropy. Li and Wang (2004) proposed a 3D cohesive isotropic damage model that uses the idea of RVE. The model of Li and Wang (2004) can model material degradation and failure due to cohesive microcrack growth. However, the use of these models is often limited by the complexity of the calculation process caused by a variety of damage mechanisms.

The concept of microplane models can be used to characterize damage orientation. The concept is based on the initial idea of slip theory of plasticity used in metal (Batdorf and Budiansky 1949) and rock-like materials (Zienkiewicz and Pande 1977). Bazant and colleagues extended the microplane model approach to describe the softening behavior of quasi-brittle materials such as concrete (Bazant and Oh 1985, Bazant and Kim 1986, Bazant and Prat 1988, Bazant et al. 1996, Bazant et al. 2000, Bazant and Jirásek 2002, Bazant and Zi 2003). This approach is different from the method that constructs constitutive models using macroscopic continuum damage mechanics, fracturing theory, or stress-strain tensors and their invariants. These microplanes may be imagined to represent damage planes or weak planes in mesoscale structures, such as layers or defects within a material (Jin et al. 2016). The microplane model describes the constitutive behavior of a material using stress and strain vectors that act in all possible orientations on the RVE in the material. This approach circumvents the limitation of stress and strain invariants (the relationship can be automatic following integration), and the macroscopic strain or stress tensors are considered to be a summation of all these vectors under the assumption of a static or kinematic constraint (Bazant et al. 1996). The advantage of the microplane model is that it is easier to make anisotropic generalizations. Microplane models can also be used to model the creep of anisotropic clay (Bazant and Kim 1986, Bazant and Prat 1987). Based on the assumption of a parallel coupling between joints and rock, Chen and Bazant (2014) presented a microplane model for the anisotropic behavior of a jointed specimen. When an anisotropic model (Li et al. 2019a) coupled with a spherocylindrical microplane constitutive model (Li et al. 2017) and Kelvin chain was introduced into finite element analysis, the numerical simulations agreed with the experimental results. The features of the microplane model, and its differences and similarities with other approaches, was described in detail by Bažant (1999) and Brocca and Bazant (2000). The concrete and isotropic rock used in classical microplane models (Bazant and Zi 2003) were characterized by 29 parameters, most of which are difficult to obtain from laboratory experiments.

The damage process of rock can be regarded as the reduction of the effective strength of an element during loading, which leads to a local stress concentration and can promote macroscopic failure. We also note that damage is anisotropic and will also depend on the initial microstructure of the rock. In this paper, the advantages of the microplane model were incorporated in a damage model based on continuum damage mechanics. The basic idea of the model is that all of the damage in each orientation of an element in the material can interact and damage occurs in one direction and is inhibited in the other directions. The relationship between the stress and strain on the microplanes also satisfies the elastic-brittle damage constitutive function used in Xu et al. (2021b), and the yield function depends on the normal and tangential strain of the microplanes. This model is proposed to characterize the anisotropic mechanical behavior, damage evolution, and failure mode of sedimentary rock in the framework of continuum mechanics.

2. Anisotropic damage-based microplane model

2.1 Brief introduction to the microplane model

It is first necessary to introduce the framework of the microplane model which has been used to simulate the mechanical behavior of quasi-brittle materials such as concrete, soil, rock, and fiber composites, etc. The model contains planes of many different orientations called microplanes (Brocca and Bazant 2000). Superimposing stress-strain vectors on these microplanes of different orientations will obtain the usual macroscopic stress and strain tensors that affect the macroscopic material behavior. The direction of a particular microplane can be imaged as the vector from the center of a sphere to its outer edge, as shown in Fig. 1a (the outer edge of the sphere is represented by the blue area in Fig. 1a). There are many advanced microplane models, such as M7 (Caner and Bazant 2013a, 2013b). However, these advanced models concentrate on the calibration and verification of experiments using many material parameters.

Because of the limitation of computing capacity, the optimal integration is performed using a regular distribution of the integration points over the spherical surface. A regular polyhedron is used to approximate the sphere (Fig. 1b). It is noted that the regular polyhedron is centrosymmetric, and so the results can be expressed as double of the integration on the hemispherical surface (Bazant and Oh 1985). One of the integrations in the microplane model based on the regular polyhedron is shown in

Fig. 1b, which has 12 vertexes and 30 edges. Therefore, the total number of integration points in the regular polyhedron shown in Fig. 1b is 2×21. As a result, only 21 partial differential equations are required to accurately describe the behavior of this element.

For a generic *kth* microplane, the microplane strain is the projection of the strain tensor as shown in

Fig. 1c. The basic hypothesis is that the strain ε_N on the microplane is the projection of the macroscopic strain tensor ε_{ij}. The relationship between the unit vector n_i, normal strain ε_N, and strain tensor ε_{ij} is given by Bazant et al. (1996):

$$\varepsilon_N = N_{ij}\varepsilon_{ij} = n_i n_j \varepsilon_{ij} \tag{1}$$

where repeated indices imply summation over $i, j = 1, 2, 3$. The similar relationship in tangential strain is given by:

$$\begin{aligned} \varepsilon_M &= M_{ij}\varepsilon_{ij} \\ \varepsilon_L &= L_{ij}\varepsilon_{ij} \\ M_{ij} &= \frac{(m_i n_j + m_j n_i)}{2} \\ L_{ij} &= \frac{(l_i n_j + l_j n_i)}{2} \end{aligned} \tag{2}$$

The rate form is selected in the present study to characterize the elastic response of the material on the microplane level as follows:

$$\begin{aligned} \dot{\sigma}_N &= E_N \dot{\varepsilon}_N \\ \dot{\sigma}_M &= E_T \dot{\varepsilon}_M \\ \dot{\sigma}_L &= E_T \dot{\varepsilon}_L \\ \sigma_T &= \sqrt{\sigma_M^2 + \sigma_L^2} \end{aligned} \tag{3}$$

where the σ_N is normal stress, σ_M and σ_L are tangential stresses, and E_N and E_T are microplane moduli related to the macroscopic elastic modulus *E* and Poisson's ratio *ν* as follows:

$$E_N = \frac{E}{1-2\nu}; E_T = \frac{(1-4\nu)}{1+\nu} E_N \tag{4}$$

Under the hypothesis of the kinematic constraint, the microplane strain is the projections of the strain tensor ε_{ij}, but the microplane stress is not equal to the projections of the macroscopic stress tensor σ_{ij}. Thus, static equilibrium is applied by the principle of virtual work with reference to the surface *Ω* of a unit sphere. The basic equilibrium equation should consider any variation, $\delta\varepsilon_{ij}$, and was introduced by Bazant et al. (1996):

$$\sigma_{ij} = \frac{3}{2\pi}\int_{\Omega}(\sigma_N N_{ij} + \sigma_M M_{ij} + \sigma_L L_{ij})d\Omega \approx 6\sum_{k=1}^{N_m}\omega_k(\sigma_N N_{ij} + \sigma_M M_{ij} + \sigma_L L_{ij})^{(k)} \qquad (5)$$

where k is the microplane number (or a chosen set of integration points representing orientations defined by unit vectors n_i), N_m is the total number of the microplanes, and ω_k is the integration weight. This means that macroscopic stress-strain relations can be derived by the summation of the contributions from the individual microplane systems.

2.2 Heterogeneity of rock

Microstructural heterogeneities induced by the size and/or shape of grains or pores affect the physical and mechanical properties of rock (Baud et al. 2005, Louis et al. 2009, Griffiths et al. 2017). Hence, either the Weibull distribution, normal distribution, or average distribution functions are usually used to generate element properties randomly and automatically to describe the physical and mechanical properties of mesoscopic rock. The Weibull distribution function has been shown to well describe the mechanical properties of heterogeneous rock (Zhou et al. 2020, Xu et al. 2021b). In this way, mesoscale numerical models are able to encompass macroscopic plasticity because the elastic modulus of the elements in the model will have a relatively narrow distribution (Liang et al. 2007, Liang et al. 2008). A smooth stress-strain curve can be obtained according to the statistical distribution. The relevant equation can be written as follows:

$$f(u) = \frac{w}{u_0}\left(\frac{u}{u_0}\right)^{w-1} e^{-\left(\frac{u}{u_0}\right)^{w}} \qquad (6)$$

where u is the scale parameter of an individual element (elastic modulus, strength, and cohesion in this paper), u_0 is parameter related to the average value of elements, and w is the heterogeneity index. The probability density distribution with different heterogeneity indices is shown in

Fig. 2. As the heterogeneity index increases, the parameter in question will have an increasingly narrower distribution of values (Fig. 2).

Different from the microplane model that applies an exponential function on each microplane to characterize the stress (σ_i) − strain (ε_i) behavior (Bazant et al. 2000), the non-linear behavior characterized by the Weibull distribution and damage criterion can simplify the constitutive relationship on the microplane (Tang 1997).

2.3 *Damage evolution of the microplane model*

The classic microplane model uses the stress-strain boundary to describe the non-linear behavior of material. The advantage of this concept is that the function relating the components of microplane stress (σ_N, σ_M and σ_L) and microplane strain (ε_N, ε_M and ε_L) can be established independently. Using this concept, the model can describe the macroscopic, anisotropic, inelastic, and nonlinear behavior of rock resulting from the micromechanical mechanisms of friction, slip, and opening of cracks. The stress boundary will not be reached at the same loading step because the stress states on each microplane are different, which provides a smooth macroscopic stress-strain relation (Li et al. 2017). However, the non-linear behavior of brittle rock in this study was described using the heterogeneity and damage constitutive equations, described in the previous section. We consider here that the brittle rock will fail when the microplane stress exceeds a threshold that depends on the microplane stress. The response of the material on the microplane is elastic when the microplane stress does not exceed the specified threshold, and the microplane stress will decrease when it exceeds the threshold. Based on this, we introduce a damage criterion to describe the mechanical behavior of the quasi-brittle material.

For tensile damage in the model, it can be considered that the element is damaged when the microplane stress satisfies the damage criterion, and that the crack propagates along the direction of this microplane. When the elements are under tension ($\sigma_N \geq 0$), the damage criterion is given by:

$$f_1 = \max[\sigma_N^k] - \sigma_{t0} \tag{7}$$

where $\max[\sigma_N^k]$ is the maximum normal stress and σ_{t0} is the tensile strength of the *kth* microplane of an element. The maximum stress of the element is the maximum of the normal stress on a *kth* microplane in all directions.

When the element is under compression ($\sigma_N < 0$), the damaged microplane can be assumed to be governed by the sliding crack model (Stevens and Holcomb 1980) and the Mohr-Coulomb law can describe the relation between the normal stress and the shear stress. For compressive and shear damage in the microplane model, it can be considered that the element is damaged when the normal stress σ_N and tangential stress σ_T on the *kth* microplane of an element satisfies the damage criterion. The equation can be written as follows:

$$f_2 = \sigma_N^k \tan\theta_f + c_0 - \sigma_T^k \tag{8}$$

where σ_N^k and σ_T^k are normal and tangential stress of the *kth* microplane of an element, respectively, and θ_f and c_0 are friction angle and cohesion, respectively. Tensile damage is preferred when the microplane system is under tension and compression simultaneously.

A geometric damage tensor based on the microplane model was discussed by Carol et al. (1991). However, damage on the microplane in this study was a scalar, and occurred when the damage criterion ($f_1 \geq 0$ or $f_2 \geq 0$) was satisfied. We consider here that the direction of microcrack propagation has only one preferred orientation. Therefore, under the framework of microplane theory, the macro damage of an element is in one direction only.

The type of damage on the microplane (tensile damage D_t and shear damage D_c) depends on which damage criterion f_1 or f_2 is satisfied first. The relationship between the elastic modulus reduction and the microplane damage is given by continuum damage mechanics:

$$E' = (1-D)E \tag{9}$$

where *E'* is the effective elastic modulus and *E* is the undamaged elastic modulus. The elastic modulus on each microplane can be divided according to Eq. (4). The damage *D* is divided into the damage resulting from tension D_t and the damage resulting from compression D_c. As shown in Fig. 3, the normal microplane stress σ_N^k increases linearly, but it will drop when the damage criterion f_1 is satisfied when the material is under tension ($\sigma_N^k \geq 0$). Under the compressive state ($\sigma_N^k < 0$), the microplane stress threshold is controlled by both the normal stress and tangential stress, and it is damaged when the function f_2 is satisfied. The gradient of microplane stress σ_N^k and strain ε_N^k is the elastic modulus E_N on the *kth* microplane. In addition, the stress or strain state is symmetrical about the center of the sphere and only half of integral points need be calculated by partial differential equations. Thus, the damaged microplane is only calculated at each step in a microplane system. Damage can be described by the *kth* microplane:

$$D_t = \begin{cases} 0 & \varepsilon_N < \varepsilon_{t0} \\ 1-\eta\left|\dfrac{\sigma_{t0}}{\varepsilon_N E_N}\right| & \varepsilon_N \geq \varepsilon_{t0} \end{cases} \tag{10}$$

$$D_c = \begin{cases} 0 & \varepsilon_T < \varepsilon_{c0} \\ 1-\eta\left|\dfrac{\sigma_{c0}}{\varepsilon_T E_T}\right| & \varepsilon_T \geq \varepsilon_{c0} \end{cases} \tag{11}$$

where η is the residual strength coefficient (RSC), which represents the magnitude of stress reduction after damage. σ_{t0} and σ_{c0} are assigned by the input parameter strength S_0. The ratio between σ_{c0} and σ_{t0} is the ratio of the compressive to tensile strength (the CT ratio). $\varepsilon_{t0}, \varepsilon_{c0}$ is the ultimate strain corresponding to the σ_{t0} and σ_{c0}.

It is reasonable to characterize the macroscopic second rank or higher rank damage tensor using a projection tensor, similar to the relation between the microplane strain and macroscopic strain tensor. As we have mentioned before, crack propagation in an element only develops along the preferred orientation. The microplane that first satisfies the damage function is considered to influence the degradation of the corresponding element mechanical parameters. Thus, the stress or strain on the microplanes is compared to each other to confirm that the element is damaged when a microplane satisfies the damage criterion. We assume that the damage on the microplane is coupled with the microplane stress and strain. However, we also assume that microplane damage (microcrack) interaction can be neglected so that tractions on the microplanes can be calculated as induced by externally applied stresses. The macroscopic damage in the numerical model is taken into account by a self-consistent method that considers the damage as embedded into the effective elastic properties.

2.4 Characterization of the anisotropy

Anisotropy in rock can be divided into inherent anisotropy and stress induced anisotropy which are widely existed in rocks(Barton and Quadros 2014). Inherent anisotropy in rocks can be caused by weak planes (preferred orientation of microcracks, bedding plane, grain boundary, etc.). Establishment of the anisotropic numerical model for granite is shown in

Fig. 4. The local micrograph of a granite block is showed in

Fig. 4a. Then we use the FracPaQ (Healy et al. 2017) to characteristize the properties such as orientations, size and spatial distribution of fractures and grain boundaries in the local micrograph (

Fig. 4b). Although the granite does not show the strong anisotropy at macroscope like shale, the result of FracPaQ quantification of fractures and grain boundary in local micrograph of granite show the correlation of direction in

Fig. 4 c. Thus, the basic tetrahedral elements in 3D numerical model can be considered as the anisotropic continuum to simulate the anisotropic properties of rock. Direction dependence of model is due to the inhomogeneous distribution of the microplane system (Huang et al. 2016). Based on this, ellipsoid is introduced to characterize the anisotropy in rocks by directionally changing the weight in the integral scheme (

Fig. 4d). Since the macroscopic stress tensor is calculated applying integration of finite number of microplanes in the frame of microplane system, each microplane will give different feedback to the stress (Bažant and Oh 1986, Li et al. 2016), and thus it can simulate the stress-induced anisotropy of rock.

An anisotropy coefficient (AC) is introduced to describe the preferred orientation in the rock. This coefficient is defined as the distance from the center of the ellipsoid to the microplane on the ellipsoid. The physical meaning of the ellipsoid can be regarded as the rock mechanical properties in different directions. The flaws are contained in an isotropic elastic material but the strength of an element is controlled by the AC. Each microplane is a unit vector $n_i^k = (n_1^k, n_2^k, n_3^k)$, so the space line corresponding to the kth microplane can be described as:

$$\frac{x}{n_1^k} = \frac{y}{n_2^k} = \frac{z}{n_3^k} \tag{12}$$

And the spatial strength of the rock element can be described as:

$$\frac{x^2}{a^2} + \frac{y^2}{b^2} + \frac{z^2}{c^2} = 1 \tag{13}$$

When $a = b = c$, the material can be considered isotropic, with $a \neq b \neq c$ defining the case of orthogonal anisotropy, and $a = b \neq c$ defining the case of transverse anisotropy. In this study, the plane crack with a preferred orientation can be regarded as a transversely isotropic material. When the orientation is changed, it can be considered that the ellipsoid is rotated clockwise around the X-axis in the OZY plane when the initial orientation θ_x changes. As

Fig. 4d shows, damage occurs more easily in the orientation of the shorter axis. The matrix of the coordinate conversion $R_x(\theta_x)$ is:

$$R_x(\theta_x) = \begin{bmatrix} 1 & 0 & 0 \\ 0 & \cos\theta_x & \sin\theta_x \\ 0 & -\sin\theta_x & \cos\theta_x \end{bmatrix} \tag{14}$$

According to Eq. (12) to Eq. (14), the *AC* of each microplane related with the θ_x is given by:

$$AC^k = \sqrt{\left(\left(x^{'}\right)^k\right)^2 + \left(\left(y^{'}\right)^k\right)^2 + \left(\left(z^{'}\right)^k\right)^2} \tag{15}$$

where the variable in the cartesian system is:

$$\begin{aligned} x^k &= \pm\frac{n_1^k abc}{\Delta} \\ y^k &= \pm\frac{n_2^k abc}{\Delta} \\ z^k &= \pm\frac{n_3^k abc}{\Delta} \\ x^{k'} &= x^k \\ y^{k'} &= \sin\theta_x \cdot z^k + \cos\theta_x \cdot y^k \\ z^{k'} &= \cos\theta_x \cdot z^k - \sin\theta_x \cdot y^k \end{aligned} \tag{16}$$

where $\Delta = \sqrt{\left(n_1^k \cdot bc\right)^2 + \left(n_2^k \cdot ac\right)^2 + \left(n_3^k \cdot ab\right)^2}$. Then, the normal stress and tangential stress of the damaged *kth* microplane can be described as:

$$\sigma_N^k = (1-D)AC^k E_N^{'} \varepsilon_N^k \tag{17}$$

$$\sigma_T^k = (1-D)AC^k E_T^{'} \varepsilon_T^k \tag{18}$$

where E_N' and E_T' are the damaged normal and tangential elastic moduli, respectively, and *D* is the damage variable on the *kth* microplane. The damage variable varies because the strength of each microplane in an element is different.

2.5 Numerical implementation of the microplane damage model

The numerical algorithm of the heterogeneous and anisotropic damage model based on the microplane model is numerically implemented into COMSOL with MATLAB. A flow chart showing the iterative steps is presented in

Fig. 5. The process of numerical implementation is as follows:

(1) A heterogeneous distribution is assigned for each element and its parameters; (a) Young's modulus E of the elements in the numerical model, and the elastic modulus E_N and E_T on the microplanes of each element, are obtained using Eq. (4); (b) the ultimate strength S_0 under compression is assigned, and the CT ratio (Xu et al. 2012) is used in the model to identify the ultimate strength under tension; (c) cohesion C_0 is assigned; and finally, (d) damage value D is given an initial value of zero.

(2) The macroscopic strain tensor ε_{ij} is decomposed into normal and tangential strains on the microplane as described by Eq. (1).

(3) The microplane stress is calculated according to Eq. (2) and Eq. (3).

(4) The damage criterion is checked using Eq. (7) and Eq. (8) to determine the damage state.

(5) All the microplanes in an element are compared and their states revised according to the microplane with the highest damage value. The elastic moduli E_N and E_T on the microplanes are calculated and updated. At the same time as updating of the elastic moduli, the microplane stress is also updated. Then, the updated normal and tangential elastic moduli after each time step need to be calculated in the program before proceding to the next step. The current microplane stress can be calculated using Eq. (3).

(6) The current macroscopic stress tensor is calculated using Eq. (5).

(7) The model stops when the total calculating step is reached.

3. Numerical simulations for anisotropic rock

3.1 Simulations of inherently anisotropy

In this section we perform numerical simulations to test whether the model can capture the mechanical behavior of materials containing an inherent anisotropy (in this case, a crack anisotropy). A damage tensor that describes the orientated cracks was developed and verified by both experiments using intact and cracked plaster specimens and simulations using the finite element method (Kawamoto et al. 1988). The cracked plaster specimens used in Kawamoto et al. (1988) had several plane cracks (see inset in Fig. 6b) and the intact specimens contained no visible cracks. The improved microplane damage model with the same dimensions as these plaster specimens (50 mm ×100 mm×300 mm) will now be used to compare the model output with these previously published experimental data. Our focus in this section is the variation in material strength due to the crack orientation, and so a precise modeling of the fracture process using the finite element method is not necessary at this stage. Further, this explicit algorithm in the finite element method is preferred to solve coupled partial differential equations. The parameters of the plaster experiments (Kawamoto et al. 1988) and the physical input parameters for the numerical model are given in Table 1. It should be noted that parameters such as strength S_0, elastic modulus E, and cohesion C_0 are the mean values from the Weibull distribution in the numerical model (Eq. (6)). Differently orientated crack angles (angle between the loading direction and crack preferred orientation) are represented by the angle θ_x. The numerical specimens were deformed at a strain rate of 1×10^{-5} s^{-1} along the direction of the maximum principal stress σ_1. The difference between the intact model and the cracked model provides the parameters of the AC, which are $a = b = c = 1$ for the intact model, and $a = b = 0.5$, $c = 1$ for the cracked model. This means that when the crack angle is $\theta_x = 0°$, the crack model has a preferred orientation in the vertical direction. The simulations show that the uniaxial compressive strength of the intact specimen is higher than the cracked specimens, and that uniaxial compressive strength decreases as a function of decreasing crack angle in the cracked specimens (Fig. 6a). We also highlight that the elastic modulus of the intact specimen is higher than that of the cracked specimens. Normalized peak strength is defined as the value obtained by dividing the uniaxial compressive strength of the cracked sample by the intact one. Normalizing the strength is required to compare our simulations with the experimental data of Kawamoto et al. (1988). Fig. 6b shows that the results of the numerical simulation are in good agreement with the experimental data of Kawamoto et al. (1988). C_n, also shown in Fig. 6b, is a crack coefficient that varies from 0 to 1 in the damage tensor based on the strain equivalence hypothesis (Kawamoto et al. 1988).

Table 1 The physical input parameters for the numerical model. The experiments on plaster are from Kawamoto et al. (1988).

Parameters	Experiments on plaster	Simulation

Strength S_0 (MPa)	--	10
Elastic modulus E (GPa)	1.11	5
Cohesion C_0 (MPa)	1.32	1
Homogeneity index w	--	5
CT ratio	--	10
Poisson's ratio ν	0.17	0.17
Friction angle θ_f (°)	8.0	8.0
RSC	--	0.01
Loading rate (s^{-1})	--	1×10^{-5}

3.2 Influence of the intermediate principal stress during true triaxial compressive loading

The effect of the intermediate principal stress σ_2 on rock strength has been investigated using a true triaxial testing apparatus (Haimson and Chang 2000, Zhenlong et al. 2019) The main difference between conventional and true triaxial testing is the ability to independently vary the magnitude of the intermediate principal stress. Hence, the anisotropic microcrack networks that can be generated during true triaxial testing are an efficient and effective way to analyze the performance of our anisotropic model. Therefore, the present numerical model is used to analyze the influence of the intermediate principal stress on rock mechanical behavior and failure. Table 2 shows the input parameters for the numerical model. The four parameters in Table 2 exert a great influence on deformation and fracturing in the numerical model. Other model parameters, such as the CT ratio, RSC, and friction angle, are the same as those listed in Table 1. We highlight that the size of the numerical model is 50 mm×50 mm×100 mm, which has the same proportion as the granite samples used in the experiments of Zhao et al. (2021) (100 mm×100 mm×200 mm), experiments that we will compare with our numerical simulations. There are different loading methods in true triaxial compression tests, such as constant stress or strain loading, constant stress rate or strain rate loading, etc. In our numerical simulations, the loading is applied along the direction of the maximum stress σ_1 (the Z-axis) at a constant displacement rate of 5×10^{-6} $m\cdot s^{-1}$. To provide the prescribed values for the intermediate principal stress σ_2 (X-axis) and the minimum principal stress σ_3 (Y-axis), we used a constant stress rate of 1.5 $MPa\cdot s^{-1}$. In the case of $\sigma_2 = 30$ MPa and $\sigma_3 = 0$ MPa, the stressing rate is 1.5 $MPa\cdot s^{-1}$ along the X-axis and the displacement rate is 5×10^{-6} $m\cdot s^{-1}$ along the Z-axis. Therefore, the stress will be constant (30 MPa) after 20 s (1 second for each calculation step), and the displacement along the Z-axis will continue to increase until the model is totally damaged or the calculation is completed. The parameters of the anisotropic coefficient are set as $a = b = c = 1$, which means that the numerical sample has no preferred orientation at the start of the simulation and the damage direction in the model will depend on the loading direction. We first compare the results of uniaxial numerical simulations with laboratory uniaxial compressive strength tests on granite in

Table 3 (Zhao et al. 2021). As shown in

Table 3, the results of the numerical simulations are in good agreement with the laboratory data of Zhao et al. (2021).

Table 2 Input parameters for numerical model used to explore the influence of the intermediate principal stress on the mechanical behavior of rock.

Strength S_0 (MPa)	Elastic modulus E (GPa)	Cohesion C_0 (MPa)	Homogeneity index w
920	47	10	5

Table 3 Physical parameters of the uniaxial experimental sample (data from Zhao et al., 2021) and the physical parameters used in the uniaxial numerical model.

Parameters	Experimental results	Numerical simulation
Peak strength (MPa)	187	192
Elastic modulus (GPa)	41	40.9
Poisson’s ratio	0.27	0.27

The true triaxial loading method described above is to make sure that $\sigma_1, \sigma_2, \sigma_3$ are applied in the same direction in a given numerical simulation. For the simulation performed at $\sigma_3 = 0$ MPa in Fig. 7a (green squares), the elastic modulus E decreased slightly when loading in the σ_2 direction stopped. Thus, the elastic modulus increased slightly as a function of increasing σ_2. The peak strength of the rock sample has the maximum value at $\sigma_2 = 60$ MPa (red triangles; Fig. 7a). The results of the numerical simulations are also compared with true triaxial experiments performed under different values of σ_2 in Fig. 7b (data for granite from Zhao et al., 2021). Although the peak strength of the simulations and experiments are quite different when $\sigma_2 = 60$ MPa, the simulations and the experiments show the same tendency as a function of increasing intermediate principal stress (Fig. 7b). We compared the peak strength verse σ_2 of microplane damage model (MPD model) with those of Mohr-Coulomb (MC) model and Drucker-Prager (DP) model, in which Mohr-Coulomb criterion and Drucker-Prager criterion are respectively used to judge the damage under compression (Zhou et al. 2020). Different from the logical scheme of microplane model, the orientation of cracks is not involved in MC model and DP model. As shown in Fig. 7c, the curve from MPD model shows that the peak strength rises firstly, then decreases after 90 MPa under the true triaxial loading (σ_3=10 MPa). Peak strength from DP model rises with the increase of σ_2, because DP criterion based on the stress invariant. Intermediate principal stress has little influence on MC model, because the intermediate principal stress σ_2 is not included in MC criterion, but σ_3 play a key role in MC model, in which peak strength is 187 MPa when σ_3=0 MPa and 226 MPa when σ_3=10 MPa. Although MPD model use the MC criterion on the microplane, the mechanical response is related to the direction of microplane. It is indicated that the effect of the intermediate principal stress under true triaxial loading is the result of anisotropic damage.

3.3 Fracture pattern during true triaxial compressive loading

To analyze the stress-induced anisotropy in rock, the fracture pattern of rock under true triaxial compression was investigated using the numerical models. The stress-strain curve for the simulation subjected to uniaxial loading ($\sigma_3 = \sigma_2 = 0$ MPa) is shown in

Fig. 7a (green squares). Snapshots of the damage evolution in this numerical model are shown in

Fig. 8a. In this uniaxial simulation, the degradation of the elastic modulus was mainly induced by tensile damage.

Fig. 8a shows snapshots of the evolution of elastic modulus and damage evolution for the numerical sample deformed under uniaxial compression ($\sigma_2 = \sigma_3 = 0$ MPa). For the elastic modulus snapshots, warm colors represent high values and cold colors represent low values. To distinguish between the two types of damage, tensile damage D_t is negative and shear damage D_c is positive in the legend of

Fig. 8 (Yuan et al. 2021). In Fig. 8a, shear damage and tensile damage occurred randomly at 80 s and grew in size up to 100 s. The stress dropped at around 100 s when the strain of the model was around 0.5%. To better observe the fracture distribution and orientation, we have filtered out the shear damage in Fig. 8. Fig. 8b shows a true triaxial simulation in which a σ_2 of 30 MPa was applied along the Y-axis. This simulation shows that the generation of damage is in the direction of the Y-axis (Fig. 8b). Using the distribution of elastic modulus, we conclude that the fracture plane is parallel to the σ_2 direction when σ_2 is applied along the Y-axis. The fracture plane is shown in gray in the schematic diagram in the bottom right image (Fig. 8b).

Fig. 8c shows the case in which a σ_2 of 30 MPa is applied along the X-axis. Although the damage evolution is quite different from the case shown in

Fig. 8b, the fracture plane is still parallel to the direction of σ_2 (i.e. along the X-axis). Furthermore, the case of $\sigma_2 = 30$ MPa (Y-axis), $\sigma_3 = 10$ MPa (X-axis), and the case of $\sigma_2 = 30$ MPa (X-axis), $\sigma_3 = 10$ MPa (Y-axis) are simulated to show the fracture pattern in

Fig. 8d and

Fig. 8e. Compared with the case of $\sigma_2 = 30$ MPa (Y-axis), $\sigma_3 = 0$ MPa (X-axis), and the case of $\sigma_2 = 30$ MPa (X-axis), $\sigma_3 = 0$ MPa (Y-axis), the numerical sample runs more time to fail and the damage is more severe with the increased minimum principal stress. However, the fracture plane composed of damage element is still approximately parallel to the direction of intermediate principal stress. In conclusion,

Fig. 8 shows that the loading direction exerts a great influence on the fracture pattern that develops in the numerical model, and that the intermediate principal stress (if $\sigma_2 > \sigma_3$) controls the direction of damage propagation, such that the damage is parallel to the direction of σ_2.

4. Discussion

4.1 Deformation of an inherently anisotropic material

Natural rocks often contain an inherent anisotropy such as bedding planes, laminations, foliations or a grain or pore shape preferred orientation. Any strength anisotropy that may be induced by such inherent anisotropy is able to be realized in our improved theoretical model based on the microplane model (Chen and Bazant 2014, Li et al. 2017) and the multi-laminate model (Sadrnejad and Shakeri 2017). In order to achieve this, we include an ellipsoidal function to increase the difference between the integration points, which directly affect the micro stress and strain in a certain orientation, in the microplane system. An element is automatically considered using the variation of damage on a microplane in this model, which is similar to the multi-laminate model (Sadrnejad and Shakeri 2017). The multi-laminate model assumes that the damage develops on the microplanes independently, and that the damage planes exist in one element and have no impact on other elements. However, only one group (i.e. two planes) of microplanes may be damaged at each loading step in this study. We assume in this study that, once a microplane is damaged, the damage evolution of the other planes is suppressed, and that this damaged microplane will control the element behavior. All the mechanical parameters, such as elastic moduli and cohesion (except the strength of the element), will degrade simultaneously once a microplane has satisfied the damage function. This assumption is applied to each tetrahedral element in the numerical model (see

Fig. 4).

Specimens containing a single crack were used to investagate the effect of crack angle on mechanical behavior in previous studies (Xu et al. 2013, Li et al. 2019b, Xu et al. 2021a, Xue et al. 2021). Barre granite and Stanstead granite are reported that maximum preferred orientation of microcracks related to the directions of lowest Young's modulus and strength (Douglass and Voight 1969). The strength of numerical specimens containing a single crack, found using the model described here, shows the same tendency as a function of crack angle (preferred orientation of material) as experiments performed on cracked plaster (Kawamoto et al. 1988) (Fig. 6b). In both the experiments and models, strength increases as the crack angle is increased from 0° to 90° (Fig. 6b). However, the strength of a sample containing a single crack will also be affected by the crack length and rock properties (Yang and Jing 2011, Le et al. 2018). The mechanical properties in different directions is realized in this study by introducing Eq. (12) and Eq. (13). Obviously, the parameters a, b, and c are an idealized form to represent the preferred crack orientation. Further, these parameters promote or inhibit the damage evolution in certain directions. As described by Eq. (9), the induced damage directly affects the elastic modulus E of the specimen. The intact specimen has a higher E than the cracked specimen, and the specimen with a crack angle of 0° has the lowest E (Fig. 6a). This means that the cracks that form in response to the loading changed the mechaincal properties of the rock. With the increase in crack angle, the ability of the material to resist elastic deformation will increase. The elastic modulus increases with the crack angle (i.e. the angle of the ellipsoid), and thus the maximum strength of a cracked specimen occurs when the crack angle is 90°. When the crack angle is 0° (

Fig. 4d), $a = b = 0.5$, $c = 1$, where a corresponds to the X-axis, b corresponds to the Y-axis and c corresponds to the Z-axis. The length from the center to the ellipsoid surface refers to how easily the microplane can satisfy the damage criterion, whereby a longer length means that the microplane is more easily damaged. Thus, the microplane system can be more easily damaged at a crack angle of 0° than at 90° under axial loading. Also, the Young's modulus of rock at 0° is lower than that at 90° (shown in

Fig. 9). Understanding the relationship between the elastic modulus and the crack angle will be helpful in predicting the mechanical behavior of a cracked rock mass. However, relationship between the numerical parameters in the equations and real physical parameters is uncertain at present due to the limitations of the currently available data.

4.2 Stress induced anisotropic damage under true triaxial loading

The fracture pattern that develops in the model is related to the minimum strength of an interface at an angle of $(90° + \varphi)/2$, where φ is the friction angle. However, the problem becomes more complicated in three-dimensions because the damage will be influenced by the stress loading path. For the constitutive relationship based on stress tensors, the fracture pattern will not change with the direction of stress since the element state is controlled only by the magnitude of the stress.

The results of true triaxial experiments are ideal to test our model, due to the crack anisotropy that develops during truly triaxial loading in these experiments. To describe the effect of the intermediate principal stress on the mechanical behavior of rock in true triaxial experiments, the constitutive relationship must necessarily include the stress tensor σ_2. The Drucker-Prager yield criterion is often used in numerical simulations to account for σ_2 (Liang et al. 2006, Pan et al. 2012). However, the nature of the stress-induced anisotropy has rarely previously been considered in this type of model. In the present model, the maximum tensile stress criterion and Mohr-Coulomb criterion are considered on the microplanes, and the application of σ_2 in the model changes the microplane strain-stress state in the loading direction. The macro stress tensor obtained from the integration of microplane stress for a particular element will influence the surrounding elements. In the direction of applied σ_2, the microplane stress increases with the value of σ_2 until it satisfies the damage criterion. Thus, the macro fracture pattern is random under uniaxial compression, but it will be parallel to the intermediate principal stress ($\sigma_2 > 0$) under true triaxial compression. Whether the σ_2 is applied along the X- or Y-axis, the damage plane is always parallel to the σ_2 direction (as shown in Fig. 8). The strength (peak stress) is the macroscopic consequence of the heterogeneous rock particles in a sample under the compressive loading. This means that some elements are damaged before the peak stress is reached and some elements remain undamaged after peak stress, which allows us to visualize the damage evolution during the numerical simulation. The maximum tensile stress criterion for the tensile state and the Mohr-Coulomb criterion for the compressive state are used to reliably analyze the damage of a particular element, and the intermediate principal stress makes no contribution to these results. The damage always occurs in a relatively weak area during loading. However, the orientation of the resultant fracture following deformation is not always the same in heterogeneous rock. The increase of the intermediate principal stress σ_2 increases the strength of rock in the loading direction, and it will influence the orientation of the damage in the microplane system. As a result, the strength (peak stress) will increase because the direction of the lowest strength has changed. The strength increases with increasing σ_2 until it reaches a certain value (60 MPa in our simulations; Fig. 7b). This is because the intermediate principal stress cannot increase the strength of microplanes in all directions. Meanwhile, the increase of σ_2 will decrease the strength of all the other microplanes. Thus, the intermediate principal stress results in a stress-induced anisotropy.

Fig. 7 shows that the intermediate principal stress effect in our numerical simulations has almost the same tendency as for true triaxial experiments performed on granite (data from Zhao et al., 2021). However, there is a slight difference in strength between the model and the expeirments when $\sigma_2 = 60$ MPa (Fig. 7b). This is because the model only has four parameters related to the mechanical properties.

The typical fracture pattern of brittle rock specimens deformed under true triaxial loading is shown in

Fig. 10a (Feng et al. 2015), in which θ is defined as the fracture angle between the normal of the fracture plane and the σ_1 direction. The fracture plane during true triaxial loading is always parallel to the direction of σ_2, which means that the loading direction has a great influence on the damage pattern. One of the advantages of the proposed numerical model is that it is able to simulate loading of the numerical specimen evenly. Meanwhile, the numerical simulations shown in

Fig. 8a and

Fig. 8b highlight that the macroscopic fractures in the model will always form parallel to the direction of σ_2. Relatively larger stresses will exceed the damage threshold of the rock along the loading direction and will promote the propagation of the damage. Thus, the fracture plane formed in the model will always be approximately parallel to σ_2, as shown in

Fig. 10. The experimental results of cumulative acoustic emission (AE) under the true triaxial test (Bai et al. 2022) is compared with numerical simulations, the purple plane based on AE events shows the potential damage plane (

Fig. 10b). In the stage of increasing σ_2, the damage plane is approximately parallel to σ_2, Bai et al. (2022) thinks the generated cracks have preferred orientation in the direction of σ_2. The numerical model presented in this paper can also show the effect of the intermediate principal stress.

5. Conclusions

We present here a microplane-based anisotropic damage model that can be used to capture the mechanical behaviour of inherently anisotropic rock and the stress-induced anisotropy that develops in isotropic rock following differential loading. In the model, the maximum tensile stress criterion and the Mohr-Coulomb criterion are used as the damage criteria for tensile and compressive damage, respectively. Each microplane can be assumed to represent cracks in a particular region (microplane system) with any orientation. The model can simulate cracks with a preferred orientation by introducing an ellipsoidal function. Because the model will decrease the elastic modulus when cracks form in the specimen, the preferred orientation means that it will more easily satisfy the damage criterion. Thus, rock will be easily damaged when the preferred orientation of cracks is parallel to the loading direction. Likewise, the rock will be stronger when the preferred orientation is perpendicular to the loading direction.

The intermediate principal stress in true triaxial loading is known to influence the direction of the resultant macroscopic fracture. As a result, the proposed microplane model is ideally suited to simulate true triaxial experiments. To do so, we only need to use the maximum tensile stress criterion and the Mohr-Coulomb criterion in the microplane model, and do not need to consider other more complex criteria that need to include stress or strain invariants. Furthermore, we show that the fracture pattern of brittle rock observed in true triaxial experiments can be reproduced by our model. Our models show that the applied loading can influence the direction of crack propagation, as seen in previous experimental studies.

The model presented in this study is based on the framework of a microplane model and uses the maximum tensile stress criterion and Mohr-Coulomb criterion to characterize how rock mechanical behavior is affected by crack orientation. However, there are currently relatively few input parameters available for the numerical model from laboratory experiments, which affects the calibration and validation of the model. Field and laboratory tests should therefore be performed to verify the rationality of the proposed model in future studies.

Acknowledgements

The work was jointly supported by National Natural Science Foundation of China (42172312, 51974062, and 52211540395) and a Royal Society-Newton Mobility Grant (IEC\NSFC\170625). M.J. Heap acknowledges support from the Institut Universitaire de France (IUF).

References

COMSOL Multiphysics® v. 5.2. cn.comsol.com. Stockholm, Sweden, COMSOL AB

Ashby MF, Sammis CG (1990) The damage mechanics of brittle solids in compression. Pure and Applied Geophysics 133: 489-521

Bai Q-s, Zhang C, Young RP (2022) Using true-triaxial stress path to simulate excavation-induced rock damage: a case study. International Journal of Coal Science & Technology 9: 49

Barton N, Quadros E (2014) Anisotropy is everywhere, to see, to measure, and to model. Rock Mechanics and Rock Engineering 48: 1323-1339

Batdorf SB, Budiansky B (1949) A mathematical theory of plasticity based on the concept of slip. Soviet Applied Mechanics 12: 1102-1112

Baud P, Louis L, David C, Rawling G, Wong T-f (2005) Effects of bedding and foliation on mechanical anisotropy, damage evolution and failure mode. Geological Society, London, Special Publications 245: 223-249

Bažant P, Oh B (1986) Efficient Numerical Integration on the Surface of a Sphere. Zeitschrift Angewandte Mathematik und Mechanik 66: 37-49

Bažant Z (1999) Size effect on structural strength: A review. Archive of Applied Mechanics 69: 703-725

Bazant Z, Caner F, Carol I, Adley M, Akers S (2000) Microplane model M4 for concrete. I: formulation with work-conjugate deviatoric stress. Journal of Engineering Mechanics 126: 944-953

Bazant Z, Jirásek M (2002) Nonlocal integral formulations of plasticity and damage: survey of progress. Journal of Engineering Mechanics 128: 1129-1239

Bazant Z, Kim J-K (1986) Creep of anisotropic clay: Microplane model. Journal of Geotechnical Engineering 112: 458-475

Bazant Z, Oh B (1985) Microplane model for progressive fracture of concrete and rock. Journal of Engineering Mechanics 111: 559-582

Bazant Z, Prat P (1987) Creep of anisotropic clay: New microplane model. Journal of Engineering Mechanics 113: 1050-1064

Bazant Z, Prat P (1988) Microplane model for brittle-plastic material: I. Theory. Journal of Engineering Mechanics 114: 1672-1688

Bazant Z, Xiang Y, Prat P (1996) Microplane model for concrete. I: Stress-strain boundaries and finite strain. Journal of Engineering Mechanics 122: 245-254

Bazant Z, Zi G (2003) Microplane constitutive model for porous isotropic rocks. International Journal for Numerical and Analytical Methods in Geomechanics 27: 25-47

Benson P, Schubnel A, Vinciguerra S, Trovato C, Meredith P, Young RP (2006) Modeling the permeability evolution of microcracked rocks from elastic wave velocity inversion at elevated isostatic pressure. Journal of Geophysical Research 111

Brocca M, Bazant Z (2000) Microplane constitutive model and metal plasticity. Applied Mechanics Reviews 53: 265-280

Browning J, Meredith P, Stuart C, Harland S, Healy D, Mitchell T (2018) A directional crack damage memory effect in sandstone under true triaxial loading. Geophysical Research Letters 45

Browning J, Meredith P, Stuart C, Healy D, Harland S, Mitchell T (2017) Acoustic characterization of crack damage evolution in sandstone deformed under conventional and true triaxial loading: Crack damage evolution in sandstone. Journal of Geophysical Research: Solid Earth 122

Caner F, Bazant Z (2013a) Microplane model M7 for plain concrete. I: Formulation. Journal of Engineering Mechanics 139: 1714-1723

Caner F, Bazant Z (2013b) Microplane model M7 for plain concrete. II: Calibration and verification. Journal of Engineering Mechanics 139: 1724-1735

Carol I, Bazant Z, Prat P (1991) Geometric damage tensor based on microplane model. Journal of Engineering Mechanics 117: 2429-2448

Cerfontaine B, Collin F (2018) Cyclic and fatigue behaviour of rock materials: review, interpretation and research perspectives. Rock Mechanics and Rock Engineering 51: 391-414

Chen X, Bazant Z (2014) Microplane damage model for jointed rock masses. International Journal for Numerical and Analytical Methods in Geomechanics 38: 1431-1452

Chow CL, Wang J (1987) An anisotropic theory of continuum damage mechanics for ductile fracture. Engineering Fracture Mechanics 27: 547-558

Daoud A, Browning J, Meredith P, Mitchell T (2020) Microstructural controls on thermal crack damage and the presence of a temperature-memory effect during cyclic thermal stressing of rocks. Geophysical Research Letters 47

David E, Brantut N, Hansen L, Mitchell T (2018) Absence of stress-induced anisotropy during brittle deformation in antigorite serpentinite. Journal of Geophysical Research: Solid Earth 123: 10616-10644

Douglass PM, Voight B (1969) Anisotropy of granites: a reflection of microscopic fabric. Geotechnique 19: 376-398

Feng X-T, Zhang X, Kong R, Wang G (2015) A novel mogi type true triaxial testing apparatus and its use to obtain complete stress–strain curves of hard rocks. Rock Mechanics and Rock Engineering 49: 1649-1662

Griffiths L, Heap MJ, Xu T, Chen C, Baud P (2017) The influence of pore geometry and orientation on the strength and stiffness of porous rock. Journal of Structural Geology 96: 149-160

Gupta I (1973) Seismic velocities in rock subjected to axial loading up to shear fracture. Journal of Geophysical Research 78: 6936-6942

Haimson B, Chang C (2000) A new true triaxial cell for testing mechanical properties of rock, and its use to determine rock strength and deformability of Westerly granite. International Journal of Rock Mechanics and Mining Sciences 37: 285-296

Healy D, Rizzo R, Cornwell D, Farrell N, Watkins H, Timms N, Gomez-Rivas E, Smith M (2017) FracPaQ: A MATLAB™ toolbox for the quantification of fracture patterns. Journal of Structural Geology 95: 1-16

Heap MJ, Dg F, Meredith P, Vinciguerra S (2010) Elastic moduli evolution and accompanying stress changes with increasing crack damage: Implications for stress changes around fault zones and volcanoes during deformation. Geophysical Journal International 183: 225-236

Heap MJ, Meyer G, Noël C, Wadsworth F, Baud P, Violay M (2022) The permeability of porous volcanic rock through the brittle-ductile transition. Journal of Geophysical Research: Solid Earth 127

Heap MJ, Vinciguerra S, Meredith P (2009) The evolution of elastic moduli with increasing crack damage during cyclic stressing of a basalt from Mt. Etna volcano. Tectonophysics 471: 153-160

Huang L, Li J, Tue NV, Němeček J, Püschel T (2016) Numerical aspects of microplane constitutive models for concrete. Applied Mathematical Modelling 41: 530-548

Jin C, Salviato M, Li W, Cusatis G (2016) Elastic microplane formulation for transversely isotropic materials. Journal of Applied Mechanics 84

Kachanov M (1982a) A microcrack model of rock inelasticity part I: Frictional sliding on microcracks. Mechanics of Materials 1: 19-27

Kachanov M (1982b) A microcrack model of rock inelasticity part II: Propagation of microcracks. Mechanics of Materials 1: 29-41

Kachanov M (1982c) Microcrack model of rock inelasticity part III: Time-dependent growth of microcracks. Mechanics of Materials 1: 123-129

Kawamoto T, Ichikawa Y, Kyoya T (1988) Deformation and fracture behaviour of discontinuous rock mass and damage mechanics theory. International Journal for Numerical and Analytical Methods in Geomechanics 12: 1-30

Lavrov A (2001) Kaiser effect observation in brittle rock cyclically loaded with different loading rates. Mechanics of Materials 33: 669-677

Lavrov A (2003) The Kaiser effect in rocks: Principles and stress estimation techniques. International Journal of Rock Mechanics and Mining Sciences 40: 151-171

Le H, Sun S, Kulatilake P, Wei J (2018) Effect of grout on mechanical properties and cracking behavior of rock-like specimens containing a single flaw under uniaxial compression. International Journal of Geomechanics 18

Li C, Bažant ZP, Xie H, Rahimi-Aghdam S (2019a) Anisotropic microplane constitutive model for coupling creep and damage in layered geomaterials such as gas or oil shale. International Journal of Rock Mechanics and Mining Sciences 124: 1365-1609

Li C, Caner F, Chau V, Bazant Z (2017) Spherocylindrical microplane constitutive model for shale and other anisotropic rocks. Journal of the Mechanics and Physics of Solids 103: 155-178

Li S, Wang G (2004) On damage theory of a cohesive medium. International Journal of Engineering Science 42: 861-885

Li S, Zhang D, Bai X, Zhang X, Chu Y, Guo K (2019b) Experimental study on mechanical properties, acoustic emission energies and failure modes of pre-cracked rock materials under uniaxial compression. Pure and Applied Geophysics 176: 4519-4532

Li W, Rezakhani R, Jin C, Zhou X, Cusatis G (2016) A multiscale framework for the simulation of the anisotropic mechanical behavior of shale. International Journal for Numerical and Analytical Methods In Geomechanics 41

Liang Z, Tang C, Zhang Y, Tianhui MA, Zhang Y (2006) 3D numerical simulation of failure process of rock. Chinese Journal of Rock Mechanics and Engineering 25: 931-936

Liang Z, Tang CA, Tang SB, Xu T, Zuo YJ (2007) Characteristics of fractal and percolation of rocks subjected to uniaxial compression during their failure process. Yantu Gongcheng Xuebao/Chinese Journal of Geotechnical Engineering 29: 1386-1391

Liang ZZ, Tang CA, Zhang YB, TANG S, MA T (2008) Three-dimensional numerical study of direct tensile fracture of rock and associated fractal. Chinese Journal of Rock Mechanics and Engineering 27: 1402-1410

Louis L, Baud P, Wong T-f (2009) Microstructural inhomogeneity and mechanical anisotropy associated with bedding in Rothbach sandstone. Pure and Applied Geophysics 166: 1063-1087

Menéndez B, Zhu W, Wong T-f (1996) Micromechanics of brittle faulting and cataclastic flow in Berea sandstone. Journal of Structural Geology 18: 1-16

Murakami S (1983) Notion of continuum damage mechanics and its application to anisotropic creep damage theory. Journal of Engineering Materials and Technology 105: 99-105

Nara Y, Kaneko K (2006) Sub-critical crack growth in anisotropic rock. International Journal of Rock Mechanics and Mining Sciences 43: 437-453

Nemat-Nasser S, Hori M (2013) Micromechanics: Overall properties of heterogeneous materials, Elsevier

O'Connell R, Budiansky B (1974) Seismic Velocities in Dry and Saturated Cracked Solids. Journal of Geophysical Research 79: 5412-5426

Pan P, Feng X, Hudson JA (2012) The influence of the intermediate principal stress on rock failure behaviour: A numerical study. Engineering Geology 124: 109–118

Pellet F, Hajdu A, Deleruyelle F, Besnus F (2005) A viscoplastic model including anisotropic damage for the time dependent behaviour of rock. International Journal for Numerical and Analytical Methods in Geomechanics 29: 941-970

Rizzo R, Healy D, Heap MJ, Farrell N (2018) Detecting the onset of strain localization using two-dimensional wavelet analysis on sandstone deformed at different effective pressures. Journal of Geophysical Research: Solid Earth 123: 10460-10478

Sadrnejad SA, Shakeri S (2017) Fabric assessment of damaged anisotropic geo-materials using the multi-laminate model. International Journal of Rock Mechanics and Mining Sciences 91: 90-103

Sammis C, Ashby M (1986) The Failure of Brittle Porous Solids Under Compressive Stress States. Acta

Metallurgica 34: 511-526

Sayers CM, Kachanov M (1995) Microcrack-induced elastic wave anisotropy of brittle rocks. Journal of Geophysical Research Solid Earth 100: 4149-4156

Sayers CM, Munster JGV (1991) Microcrack-induced seismic anisotropy of sedimentary rocks. Journal of Geophysical Research: Solid Earth 96: 16529-16533

Sayers CM, Munster JGV, King MS (1990) Stress-induced ultrasonic anisotrophy in Berea sandstone. International Journal of Rock Mechanics & Mining Sciences & Geomechanics Abstracts 27: 429-436

Schubnel A, Benson P, Thompson B, Hazzard J, Young RP (2006) Quantifying damage, saturation and anisotropy in cracked rocks by inverting elastic wave velocities. Pure and Applied Geophysics 163: 947-973

Schubnel A, Guéguen Y (2003) Dispersion and anisotropy of elastic waves in cracked rocks. Journal of Geophysical Research: Solid Earth 108

Shao J, Chau K, Feng X-T (2006) Modeling of anisotropic damage and creep deformation in brittle rocks. International Journal of Rock Mechanics and Mining Sciences 43: 582-592

Shirole D, Hedayat A, Ghazanfari E, Walton G (2020) Evaluation of an ultrasonic method for damage characterization of brittle rocks. Rock Mechanics and Rock Engineering 53: 2077-2094

Stevens J, Holcomb D (1980) Theoretical investigation of the sliding crack model of dilatancy. Journal of Geophysical Research 85: 7091-7100

Stuart CE, Meredith PG, Murrell SAF, Munster JGV (1993) Anisotropic crack damage and stress-memory effects in rocks under triaxial loading. International Journal on Rock Mechanics and Mining Sciences & Geomechanical Abstracts 30: 937-941

Tang C (1997) Numerical simulation of progressive rock failure and associated seismicity. International Journal of Rock Mechanics and Mining Sciences 34: 249-261

Wu X, Baud P, Wong T-f (2000) Micromechanics of compressive failure and spatial evolution of anisotropic damage in Darley Dale sandstone. International Journal of Rock Mechanics and Mining Sciences 37: 143-160

Xu L, Gong F, Luo S (2021a) Effects of pre-existing single crack angle on mechanical behaviors and energy storage characteristics of red sandstone under uniaxial compression. Theoretical and Applied Fracture Mechanics 113: 102933

Xu T, P.G R, Wasantha PLP, Zhao J, Tang CA, Zhu W (2013) Influence of the geometry of partially-spanning joints on mechanical properties of rock in uniaxial compression. Engineering Geology 167: 134–147

Xu T, Tang CA, Zhao J, Li LC, Heap MJ (2012) Modelling the time-dependent rheological behaviour of heterogeneous brittle rocks. Geophysical Journal International 189: 1781-1796

Xu T, Yuan Y, Heap MJ, Zhou G-L, Perera MSA, Ranjith PG (2021b) Microwave-assisted damage and fracturing of hard rocks and its implications for effective mineral resources recovery. Minerals Engineering 160

Xue Y, Xu T, Zhu W, Heap MJ, Heng Z, Wang X (2021) Full-field quantification of time-dependent and -independent deformation and fracturing of double-notch flawed rock using digital image correlation. Geomechanics and Geophysics for Geo-Energy and Geo-Resources 7

Yang S-Q, Jing H-W (2011) Strength failure and crack coalescence behavior of brittle sandstone samples containing a single fissure under uniaxial compression. International Journal of Fracture 168: 227-250

Yuan Y, Xu T, Heap MJ, Meredith PG, Yang T, Zhou G (2021) A three-dimensional mesoscale model for progressive time-dependent deformation and fracturing of brittle rock with application to slope stability. Computers and Geotechnics 135

Zhao XG, Wang J, Cai M, Su G (2021) Influence of intermediate principal stress on the strainburst characteristics of beishan granite with consideration of end effect. Rock Mechanics and Rock Engineering 54: 4771-4791

Zhenlong S, Yin G, P.G R, Li M, Huang J, Liu C (2019) Influence of the intermediate principal stress on sandstone failure. Rock Mechanics and Rock Engineering 52: 3033-3046

Zhou GL, Xu T, Heap MJ, Meredith PG, Mitchell TM, Sesnic ASY, Yuan Y (2020) A three-dimensional numerical meso-approach to modeling time-independent deformation and fracturing of brittle rocks. Computers and Geotechnics 117: 103274

Zienkiewicz O, Pande G (1977) Time dependent multilaminate model of rocks—A numerical study of deformation and failure of rock masses. International Journal for Numerical and Analytical Methods in Geomechanics 1: 219-247

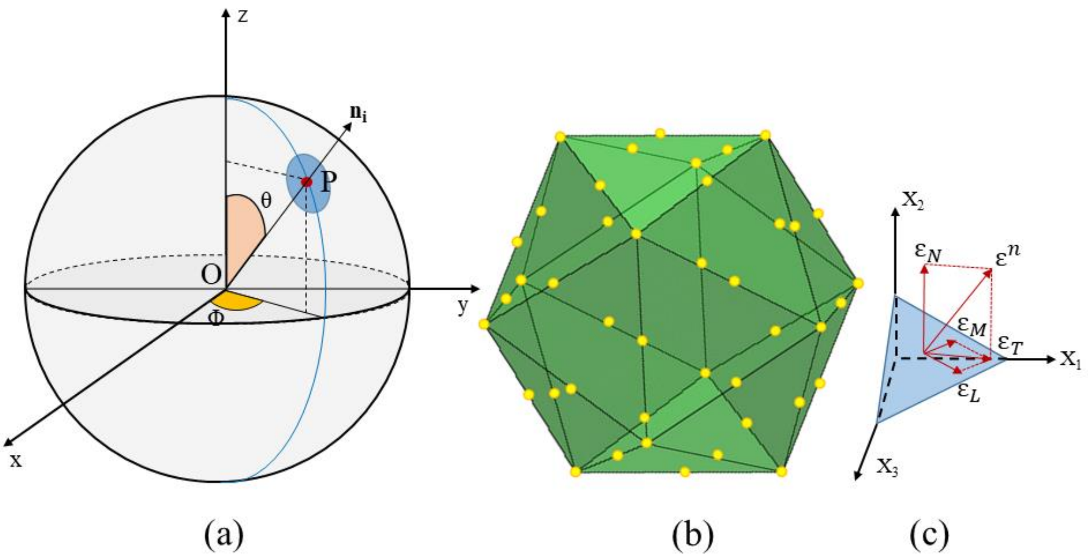

Fig. 1 The microplane system. (a) Spatial direction of the microplane (blue area). (b) For the case of 2×21 integration points, the regular icosahedron is shown in green, and the yellow points (12 vertexes and 30 midpoints of edges) represent the microplanes around an element in the material. (c) For *k*th microplane, strain vector ε^n is composed of normal strain ε_N and tangential strain ε_T in the local coordinate system.

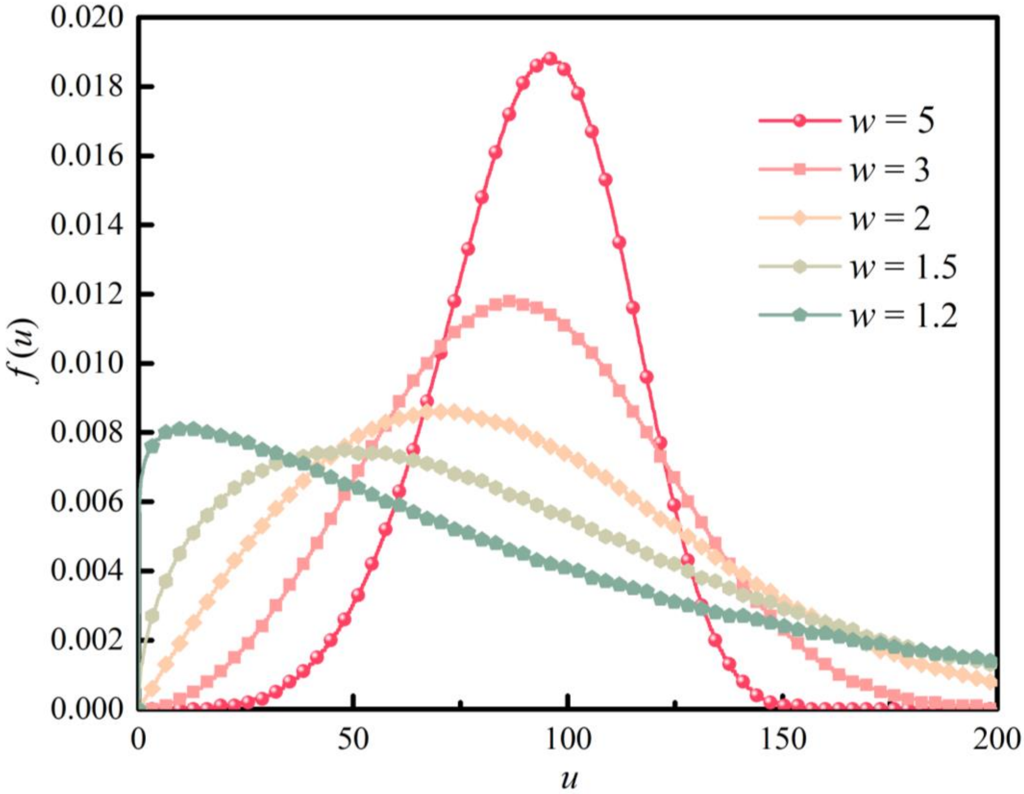

Fig. 2 Probability density distribution for scale parameter u with different heterogeneity indices w (1.2, 1.5, 2, 3, and 5).

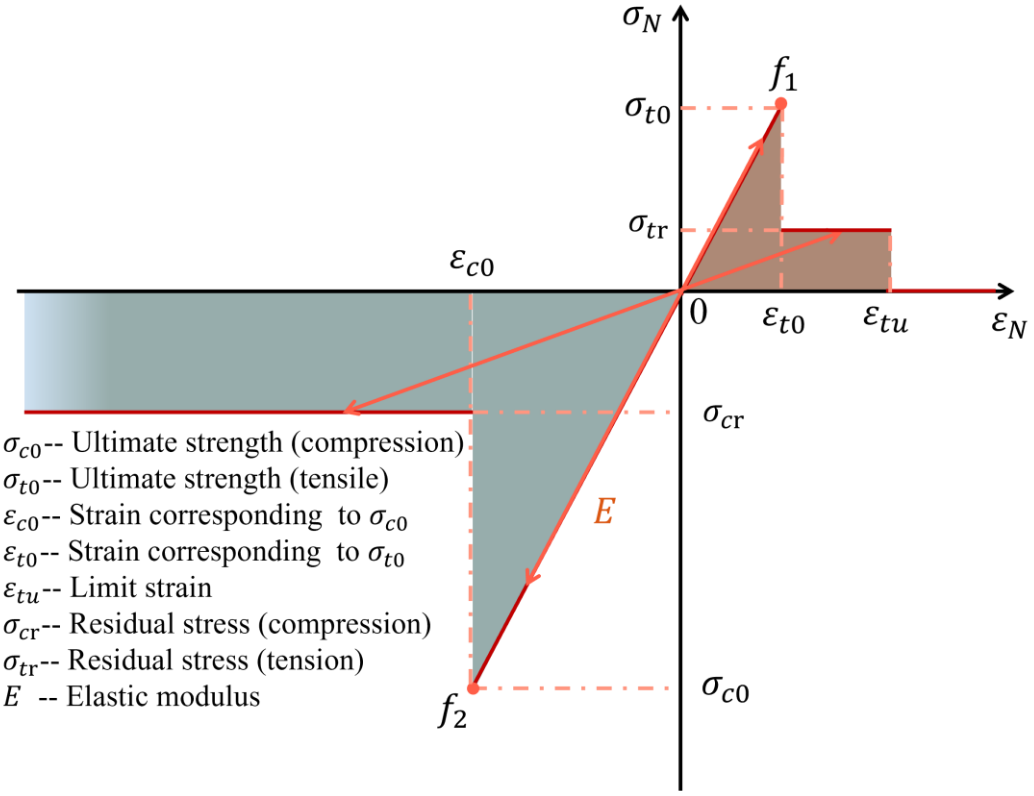

Fig. 3 Damage constitutive relationship of microplane model used in this study.

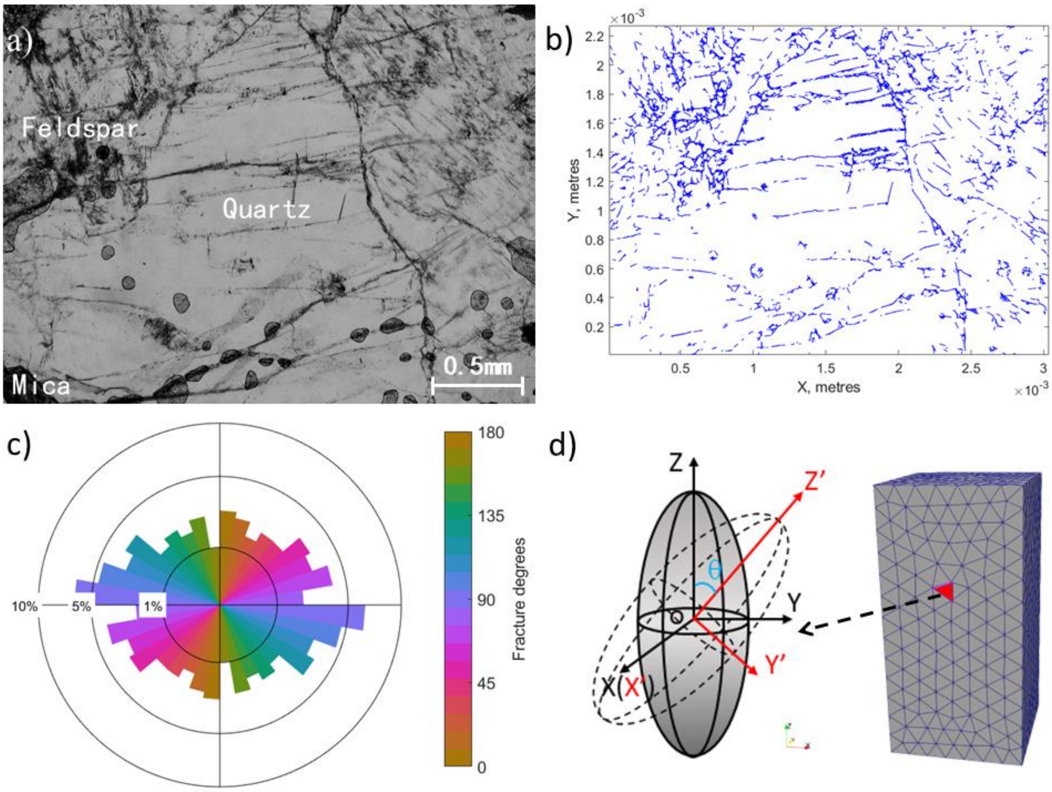

Fig. 4 Establishment of anisotropic numerical model at micro- and macro- scale. (a) Thin section of granite. (b) The trace of the microfractures and grain boundaries generated by FracPaQ. (c) Quantifying angles and proportion of the fracture pattern in micrograph. (d) An ellipsoid for the tetrahedron element in the 3D model to characterize the anisotropy of rock.

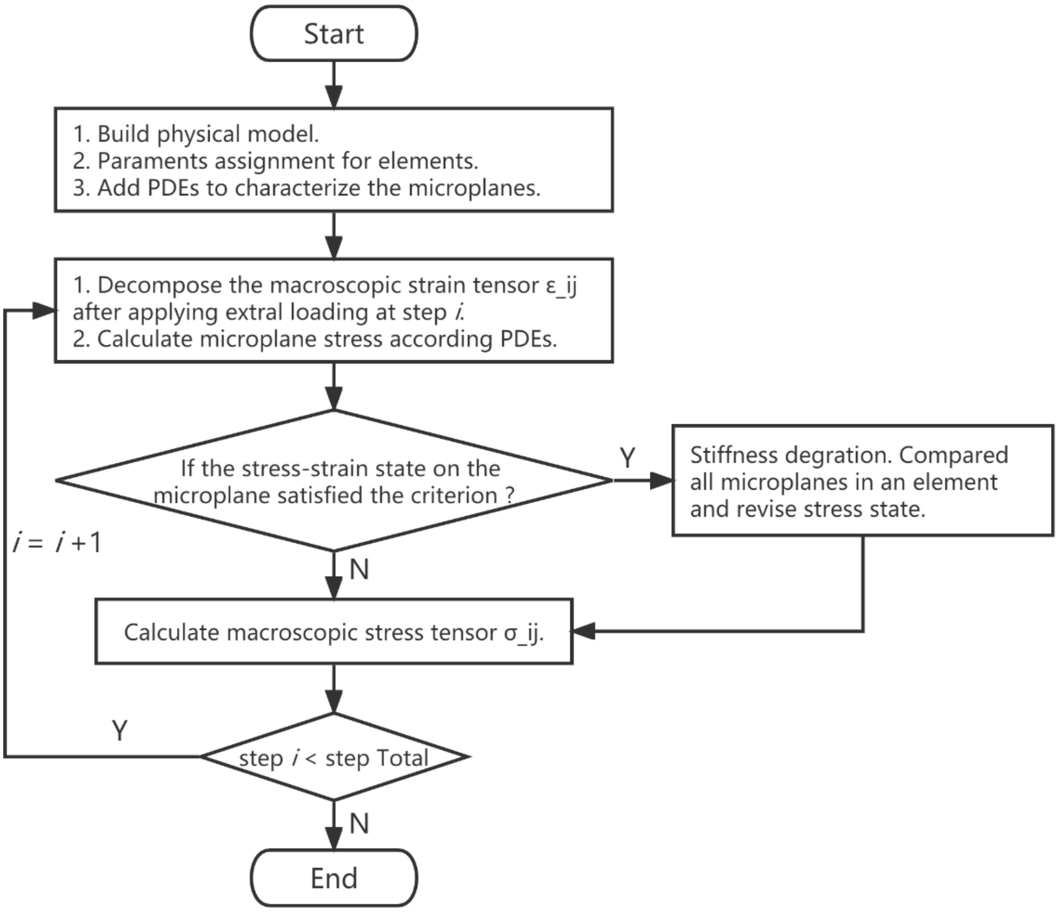

Fig. 5 Flow chart of the microplane-based anisotropic damage model developed in this study.

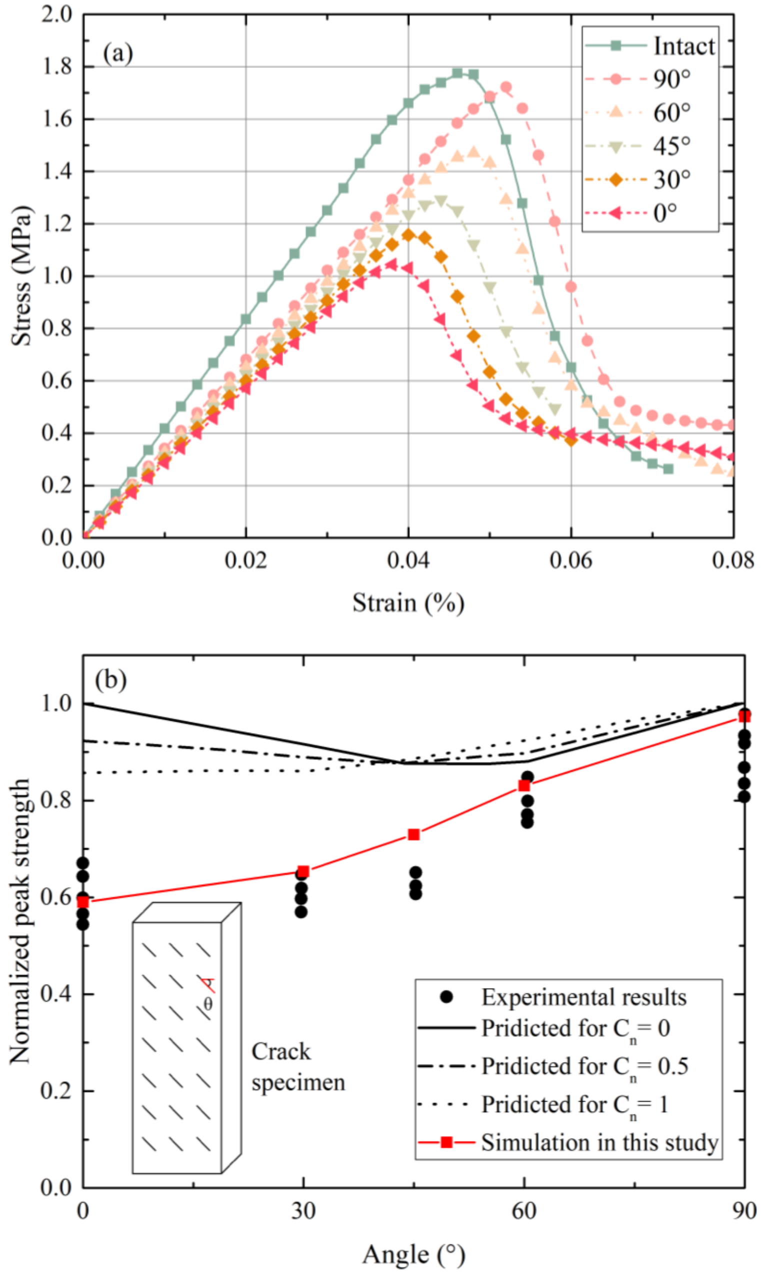

Fig. 6 Numerical simulations of intact and cracked specimens with a preferred orientation. (a) Stress-strain curves of the intact and cracked specimens from the numerical simulations (angle is the crack angle). (b) Normalized peak strength of the cracked specimens as a function of crack angle. The experimental results are shown as black circles (data from Kawamoto et al., 1988) and the results of the numerical simulations (this study) are shown as red squares. Solid, dot-dashed, and dotted lines are predictions from the damage tensor based on the strain equivalence hypothesis (Kawamoto et al., 1988).

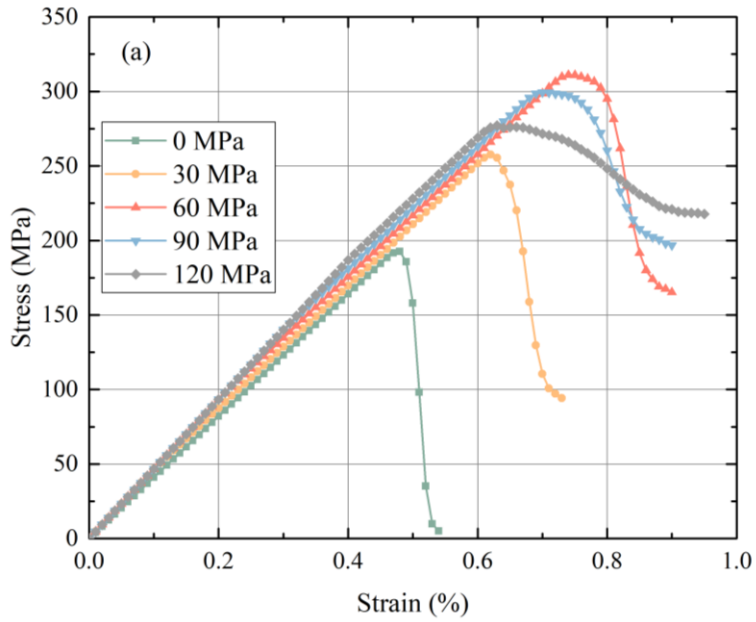
(a)
Stress (MPa)
Strain (%)
0 MPa
30 MPa
60 MPa
90 MPa
120 MPa

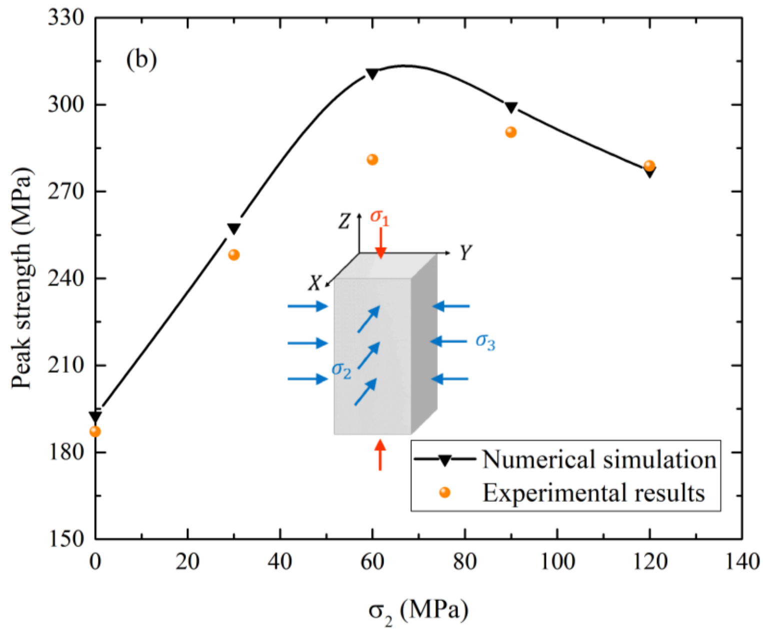
(b)
Peak strength (MPa)
σ2 (MPa)
Z
Y
X
σ1
σ2
σ3
Numerical simulation
Experimental results

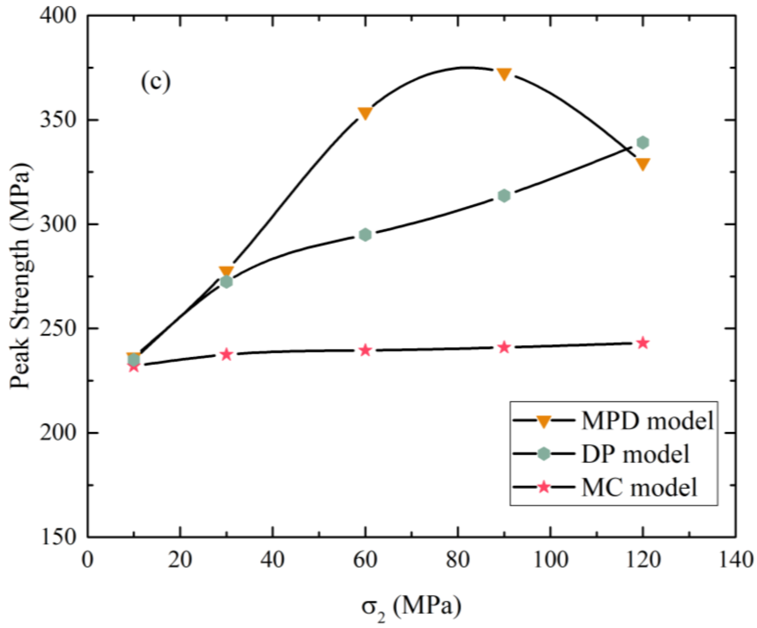

Fig. 7 Results of the true triaxial numerical simulations performed for this study. (a) Stress-strain curves for numerical samples deformed under true triaxial conditions using different values of σ_2. (b) Peak strength as a function of σ_2 for the experiments shown in (a) ($\sigma_3 = 0$ MPa). The peak stresses from our simulations (black triangles) are compared with experimental data for granite from Zhao et al. (2021) (orange circles). (c) Peak strength varied with σ_2 of different model under true triaxial loading (σ_3= 10 MPa).

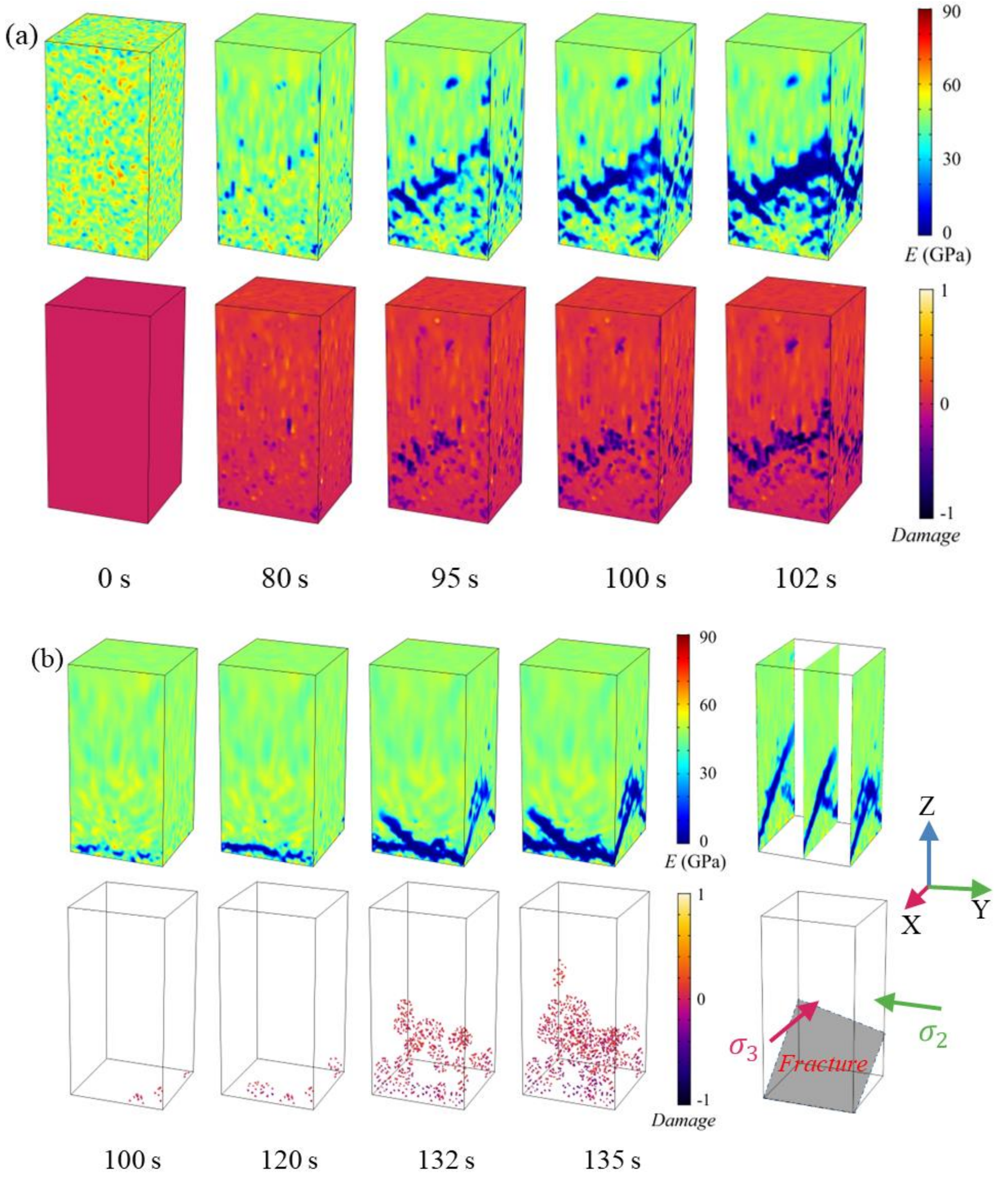

(a)
90
60
30
0
E (GPa)
1
0
-1
Damage
0 s
80 s
95 s
100 s
102 s
(b)
90
60
30
0
E (GPa)
1
0
-1
Damage
Z
X
Y
σ3
σ2
Fracture
100 s
120 s
132 s
135 s

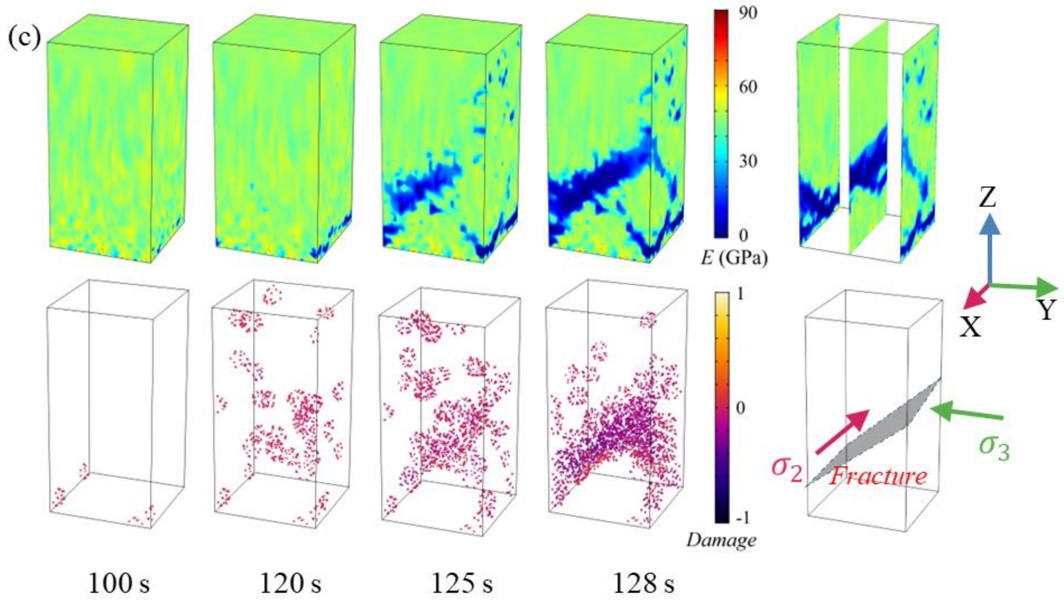
(c)
90
60
30
0
E (GPa)
1
0
-1
Damage
Z
X
Y
σ2
σ3
Fracture
100 s
120 s
125 s
128 s

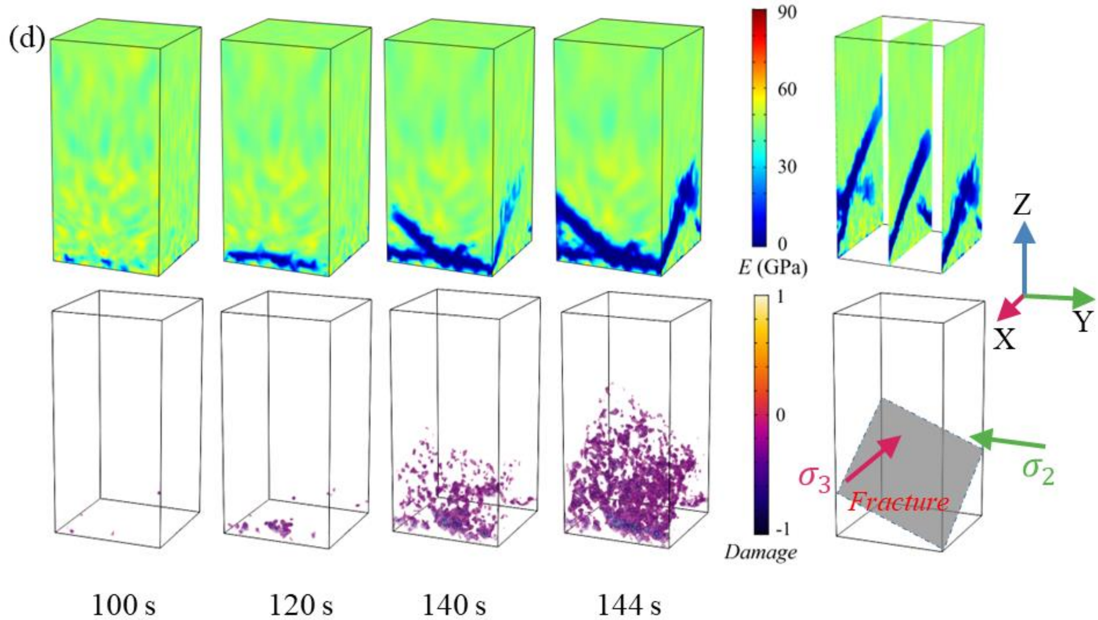
(d)
90
60
30
0
E (GPa)
1
0
-1
Damage
Z
X
Y
σ3
σ2
Fracture
100 s
120 s
140 s
144 s

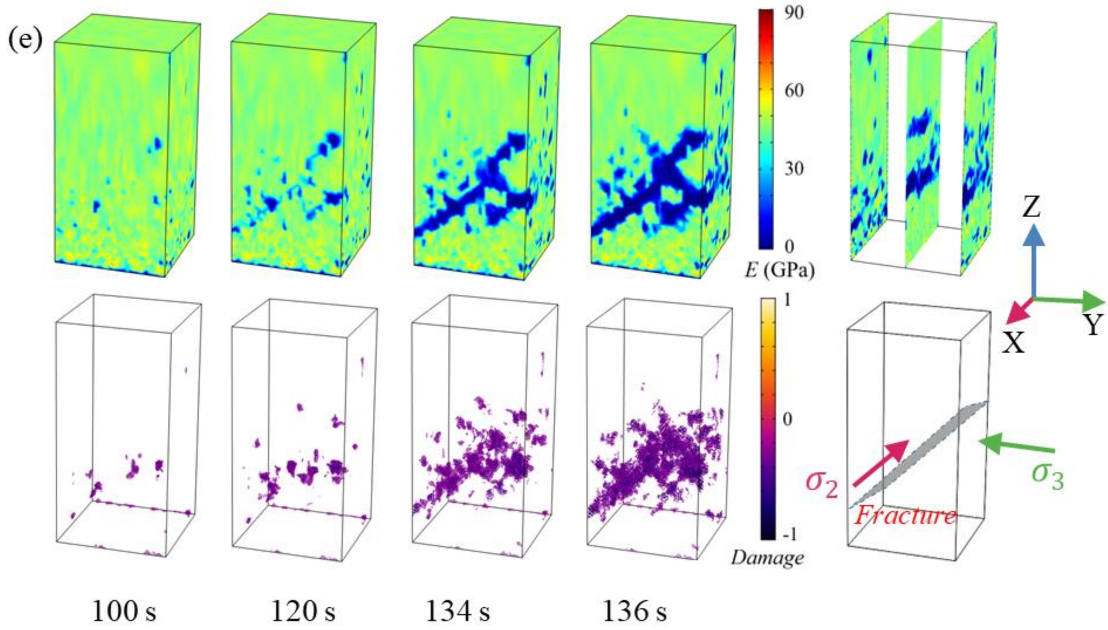

Fig. 8 Elastic modulus E and damage D evolution for the numerical simulations performed under different values of σ_2. (a) The case of $\sigma_2 = \sigma_3 = 0$ MPa. (b) The case of $\sigma_2 = 30$ MPa (Y-axis) and $\sigma_3 = 0$ MPa (X-axis). (c) The case of $\sigma_2 = 30$ MPa (X-axis) and $\sigma_3 = 0$ MPa (Y-axis). (d) The case of $\sigma_2 = 30$ MPa (Y-axis) and $\sigma_3 = 10$ MPa (X-axis). (e) The case of $\sigma_2 = 30$ MPa (X-axis) and $\sigma_3 = 10$ MPa (Y-axis).

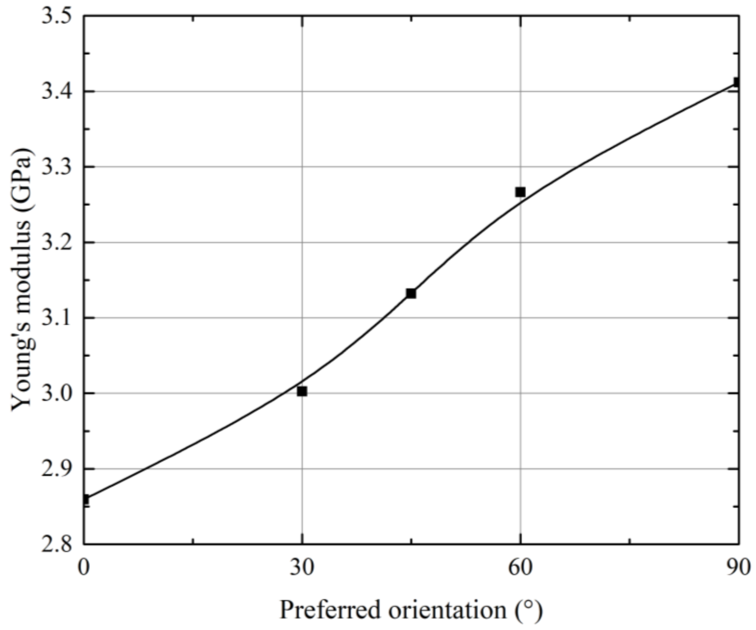

Fig. 9 Young’s modulus varied with preferred orientation of microcracks in model

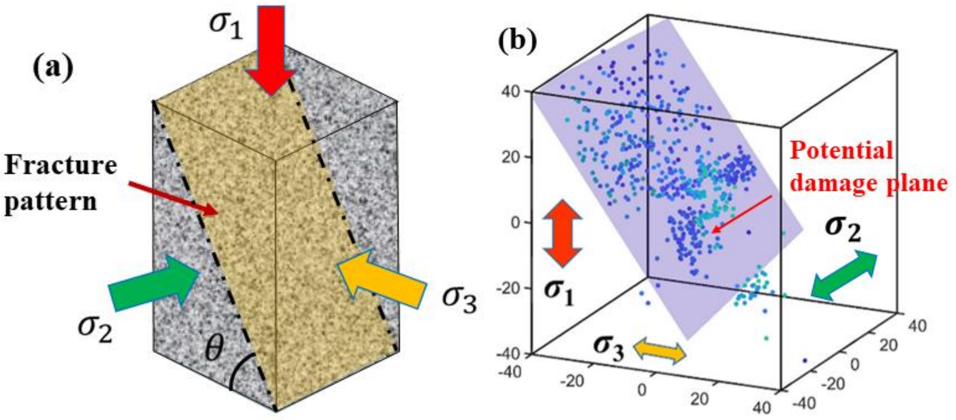

Fig. 10 Orientations of rock fracture pattern in experiments. (a)Typical fracture pattern under true triaxial compressive loading (Feng et al. 2015). (b)Cumulative acoustic emission locations of rock in true triaxial test (Bai et al. 2022).